Fermi surface of a disordered Cu-Al-alloy single crystal studied by high-resolution Compton scattering and electron diffraction

J. Kwiatkowska and F. Maniawski
The H. Niewodniczański Institute of Nuclear Physics, Radzikowskiego 152, 31-342 Krakow, Poland

I. Matsumoto, H. Kawata, and N. Shiotani
Institute of Materials Structure Science, High Energy Accelerator Research Organization, Tsukuba, Ibaraki 305-0801, Japan

L. Lityńska
Institute of Metallurgy and Materials Science of the Polish Academy of Sciences, Reymonta 25, 30-059 Cracow, Poland

S. Kaprzyk
Department of Physics, Northeastern University, Boston, Massachusetts 02115, USA
and AGH University of Science and Technology, Al. Mickiewicza 30, Cracow, Poland

A. Bansil
Department of Physics, Northeastern University, Boston, Massachusetts 02115, USA
(Received 16 March 2004; published 23 August 2004)

We have measured high resolution Compton scattering profiles for momentum transfer along a series of 28 independent directions from $Cu_{0.842}Al_{0.158}$ disordered alloy single crystals with normals to the surfaces oriented along the [100], [110], and [111] directions. The experimental spectra are interpreted via parallel first-principles KKR-CPA (Korringa-Kohn-Rostoker coherent-potential approximation) computations of these directional profiles. The Fermi surface determined by inverting the Compton data is found to be in good agreement with the KKR-CPA predictions. An electron diffraction study of the present $Cu_{0.842}Al_{0.158}$ sample is additionally undertaken to gain insight into short-range ordering effects. The scattering pattern displays not only the familiar diffuse scattering peaks, but also shows the presence of weak streaks interconnecting the four diffuse scattering spots around the (110) reciprocal lattice points. This study provides a comprehensive picture of the evolution of the shape of the Fermi surface of Cu with the addition of Al. Our results are consistent with the notion that Fermi surface nesting is an important factor in driving short-range ordering effects in disordered alloys.

DOI: 10.1103/PhysRevB.70.075106 PACS number(s): 71.18.+y, 71.20.Gj, 71.23.−k, 41.60.Ap

I. INTRODUCTION

It has become possible in recent years to map the full three-dimensional (3D) Fermi surface (FS) of wide classes of materials via high-resolution Compton scattering and positron annihilation (two-dimensional angular correlation or the 2D-ACAR) experiments.[1–11] Unlike traditional spectroscopic techniques which involve transport measurements, Compton and 2D-ACAR experiments do not require long electron mean free paths and are thus particularly well suited for investigating disordered alloys. Studies of some ordering phenomena in metallic disordered alloys and compounds, which are thought to be driven by geometry of the FS, have thus been reinvigorated.[2,8–10] An early discussion of the importance of the FS geometry in producing signatures in screening or susceptibility related phenomena in the electron gas is given by Kohn.[12] The effect can be understood by considering the familiar wave-vector dependent dielectric constant or the generalized susceptibility in the random phase approximation, which contains the characteristic factor

$$H(\mathbf{q}) = -\sum_{\mathbf{k}} \frac{f(\varepsilon_{\mathbf{k}+\mathbf{q}}) - f(\varepsilon_{\mathbf{k}})}{\varepsilon_{\mathbf{k}+\mathbf{q}} - \varepsilon_{\mathbf{k}}}, \tag{1}$$

where $\varepsilon_{\mathbf{k}}$ is the energy of electron in state $\boldsymbol{k}$ and $f(\varepsilon_{\mathbf{k}})$ is Fermi-Dirac function, and for simplicity band indices have been suppressed. Equation (1) makes it clear that the presence of nesting features in the FS, i.e., of two approximately parallel FS sheets separated by a constant distance $\boldsymbol{q}_0$, will in general induce a large response in $H(\boldsymbol{q})$ and hence in the susceptibility at $\boldsymbol{q}=\boldsymbol{q}_0$.

A note should be made of the work of Lomer,[13,14] who seems to be the first to invoke the nesting of specific FS sheets to account for antiferromagnetic ordering in chromium. Tachiki and Teramoto[15] argued that the existence of parallel FS sheets perpendicular to the [110] direction is essential for stabilizing the ordered CuAu II structure. Clapp and Moss[16,17] and Moss and Clapp[18] discussed short-range ordering in disordered binary alloys and related the position of diffuse scattering of x-rays, electrons and neutrons to the nesting singularity in $H(\boldsymbol{q})$. Moss[19] further proposed a method to caliper the distance between the flat parts of the FS from the position of the diffuse scattering peaks. A similar conclusion was reached by Gyorffy and Stocks[20] using a density-functional approach. We emphasize that in principle nesting features of the FS will yield not only diffuse scattering spots but also more extended images of the nesting portions of the FS. Matsumoto *et al.*[2] have recently mapped the 3D FS of disordered $Cu_{0.725}Pd_{0.275}$, which is well known to exhibit short-range ordering effects, and confirmed the pres-

ence of a pair of parallel FS sheets and determined the length of the nesting vector to be in very good agreement with that obtained from the positions of diffuse scattering peaks. Finally, Dugdale *et al.*[9] implicate a particular nesting FS sheet for the observed modulated magnetic structure in a study of $RuNi_2B_2C$.

With regard to relevant work on Cu-Al alloys, short-range ordering in the disordered phase has been investigated by x-ray diffuse scattering in the past.[21–23] In this way, Scattergood *et al.*[22] obtained the length of the nesting vector along the [110] direction, $2k_{F110}$, as a function of Al content. Measurements of the FS radii, k_{F100}, k_{F110}, and the neck radius k_{Neck} have been carried out via one-dimensional angular correlation of positron annihilation radiation (1D-ACAR).[24–27] These results indicate that the increase of k_{F100} is slightly larger than that of k_{F110} when Al content increases, thus suggesting the possibility of flattening of the FS in the [110] direction. Samsel-Czekała *et al.*[11] reported Compton scattering and Korringa-Kohn-Rostoker–coherent potential approximation (KKR-CPA) studies of $Cu_{0.9}Al_{0.1}$. They measured eight directional Compton profiles and employed a method which uses radon transformation to reconstruct the 3D momentum density. Applying Lock-Crisp-West (LCW) folding procedure to the obtained 3D momentum density they presented the (100), (110), and (111) FS sections. The results are, however, not focused on flattening of the FS in the [110] direction. Asonen *et al.*[28] carried out angle-resolved photoemission studies on $Cu_{0.9}Al_{0.1}$ and $Cu_{0.87}Al_{0.13}$ together with KKR-CPA computations of the band structure and the FS. On the whole, various aforementioned measurements, although consistent with one another within experimental resolution, are somewhat scattered in nature and do not provide a conclusive picture concerning the evolution of the shape of the FS of Cu with the addition of Al.

With this motivation, our goal in this article is to obtain a comprehensive map of the FS of Cu-Al alloys and of the associated changes in the shape of the FS with the addition of Al to Cu. To this end, we have undertaken an extensive high resolution Compton scattering study of a single crystal of $Cu_{0.842}Al_{0.158}$ and obtained cross-sections of the FS in the (100) and (110) planes in the Brillouin zone. The experimental results on $Cu_{0.842}Al_{0.158}$ are compared and contrasted with the corresponding first-principles KKR-CPA theoretical predictions as well as with the experimental FS maps in Cu and CuPd alloys. Moreover, in order to gain insight into short-range ordering effects, we have carried out electron diffraction measurements on the same single crystal and identified not only splitting of diffuse scattering around the (110) reciprocal lattice points, but we have also observed weak streaks interconnecting the diffuse spots in the scattering pattern. On the whole, our results provide a consistent picture of the evolution of the FS of Cu with the addition of various solutes and the presence of short-range order as being driven via nesting properties of the FS.

II. EXPERIMENT

A single crystal of $Cu_{0.842}Al_{0.158}$ was grown from the melt by a modified Bridgman method in a resistance-heated vacuum furnace. After the crystallization process, the ingot was slowly cooled to 400 °C at a rate of about 20 °C/h and subsequently furnace-cooled down to room temperature. The final composition of the alloy was determined by atomic absorption spectrometry. Electron and x-ray diffraction confirmed that there was no evidence of other phases being present in the crystal. The thin foil for electron diffraction studies was obtained by twin-jet electropolishing in nitric acid (30%)/methanol solution at −30 °C after standard mechanical and chemical thinning processes. Care was taken not to heat or bend the specimen in the process.

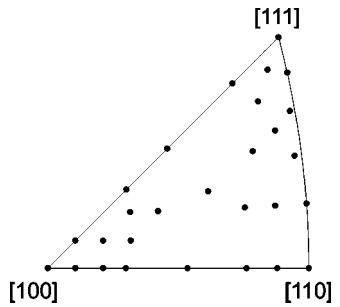

FIG. 1. Stereographic plot of the 28 directions along which the Compton profiles of $Cu_{0.842}Al_{0.158}$ were measured.

The existence of short-range ordering was investigated via observation of diffuse scattering by electron diffraction using a transmission electron microscope (Philips CM20) operated at 200 keV. The diffuse scattering spots were very weak and these were detectable only on film after prolonged exposure. It should be noted that the specimens were not subjected to any additional treatment such as annealing at elevated temperatures, quenching, or cold-work, which would affect the state of short-range ordering.

The samples for Compton scattering measurements were slices of 1.5 mm thickness with normals to the surfaces oriented along the [100], [110], and [111] directions. The Compton profiles were measured at the PF-AR NE1A1 beamline of the KEK—The High Energy Accelerator Research Organization, where the incident beam of 60 keV x-rays is available with a rate of 1.5×10^{13} photons/s. The Compton spectrometer is unique in design and consists of four independent analyzing systems arranged on the surface of a cone that provides a scattering angle of 160° to all four analyzing systems.[29] Two of these analyzing systems were used for the present experiment, one in the horizontal and the other in the vertical position as viewed from the base of the cone. A total of 28 independent directional profiles were measured along the directions shown in Fig. 1.

The overall instrumental resolution was 0.13 atomic units (a.u.) in full width at half maximum. The total accumulated counts under each profile are about 2×10^8. The measured profiles were corrected for the necessary energy dependent corrections such as absorption, detector and analyzer efficiency, and scattering cross-section. The contribution of double scattering events was estimated by a Monte Carlo simulation programmed originally by Sakai.[30] The ratio of the total intensity of double scattering to single scattering events is estimated to be 2.5%.[52] The valence electron profiles were obtained by subtracting the theoretical core electron contribution from the corrected profiles.

III. RECONSTRUCTION

In a Compton scattering experiment one measures the so-called Compton profile

$$J(p_z) = \int\int \rho(\mathbf{p}) dp_x dp_y, \tag{2}$$

where p_z is taken along the direction of the x-ray scattering vector and

$$\rho(\mathbf{p}) = (2\pi)^{-3} \sum_i \left| \int \psi_i(\mathbf{r}) \exp(-i\ \mathbf{p}\cdot\mathbf{r}) d\mathbf{r} \right|^2 \tag{3}$$

is the ground-state momentum density of the electron system, expressed in terms of the electron wave functions ψ_i, where we have implicitly invoked an independent particle model. The summation in Eq. (3) extends over the occupied states. Thus the Compton profile contains signatures of the FS breaks in the underlying $\rho(\mathbf{p})$. These FS signatures in $J(p_z)$ are however rendered less obvious by the presence of the double integral in Eq. (2). One traditional way to approach the problem is to "reconstruct" the full 3D function $\rho(\mathbf{p})$ from a suitable set of profiles measured along a series of judiciously chosen directions. Our specific scheme for reconstruction has been described at length elsewhere.[3] Briefly, we first obtain the reciprocal form factor

$$B(\mathbf{r}) = \int \rho(\mathbf{p}) \exp(-i\ \mathbf{p}\cdot\mathbf{r}) d\mathbf{p}. \tag{4}$$

It is straightforward to show that $B(\mathbf{r})$ along a specific real-space direction can be obtained by a 1D Fourier transform of the profile along the same direction. For example

$$B(0,0,z) = \int J(p_z) \exp(-i\ p_z\ z) dp_z. \tag{5}$$

By measuring $J(p_z)$, with p_z set along many different crystal directions, $B(\boldsymbol{r})$ can be computed along corresponding lines parallel to p_z in real space. An interpolation then yields $B(\boldsymbol{r})$ throughout the $\boldsymbol{r}$-space. The back Fourier transformation of $B(\mathbf{r})$ finally gives the 3D $\rho(\mathbf{p})$ from Eq. (4). Such a direct Fourier transform method was applied by Suzuki *et al.*[31] to reconstruct the 3D electron-positron pair momentum density in Ti and Zr from 2D-ACAR spectra. Later, the method was employed to reconstruct the 3D unpaired spin momentum density in Fe,[32] 3D momentum density in Li,[3] and in Cu-Pd.[2]

For the present measurements the total standard deviation σ can be shown to be given by

$$\sigma = \sqrt{N_0} + 0.005 \times N_0. \tag{6}$$

The second term on the right side above reflects the effects of the readout system and the nonuniformity of the photostimulable phosphor in the image plate; see, Ito and Amemiya[33] for details. The error propagation calculations used in this paper are the same as those used by Tanaka *et al.*[3]

IV. THEORETICAL KKR-CPA COMPUTATION OF MOMENTUM DENSITY

The electronic structure of disordered $Cu_{0.842}Al_{0.158}$ alloy was computed within the all-electron charge self-consistent KKR-CPA framework and is parameter-free. The underlying KKR-CPA methodology is described in Refs. 34–38. From these computations a lattice constant of 6.879 a.u. was found for the alloy by minimizing the total energy using 1183 $\boldsymbol{k}$-points in the irreducible Brillouin zone within a spherical muffin-tin geometry. The relevant Green's function formulation for treating the momentum density is given in Refs. 39 and 40. Exchange-correlation effects were incorporated within the von Barth-Hedin local density approximation.[41] Other more satisfactory forms of the exchange-correlation functional could of course be used in the process of obtaining the self-consistent crystal potential. However, we expect the conclusions of this paper to be robust to such uncertainties inherent in the band theory framework.

In order to obtain the Compton profiles, the momentum density $\rho(\mathbf{p})$ was first evaluated over a fine mesh of 1183 $\times$ 2421 $\boldsymbol{p}$ points covering momenta up to $p_{\max} \sim 20.0$ a.u. This fine mesh, which corresponds to 1183 *ab initio* $\boldsymbol{k}$-points in the irreducible 1/48th of the Brillouin zone, with each $\boldsymbol{k}$-point translated to obtain 2421 $\boldsymbol{p}$-points using the reciprocal lattice vectors, is sufficient to properly treat the FS breaks and the rather long range of the momentum density. Compton profiles for scattering vectors along the set of 28 directions measured experimentally were then computed by evaluating the integral of Eq. (2) over a momentum mesh of 0.001 a.u. The accuracy of the computed profiles is about one part in 10^4. For comparison with the experiment, the 28 theoretical profiles were convoluted with the experimental resolution of 0.13 a.u. and then treated in a manner identical to that used for treating the 28 experimental profiles.

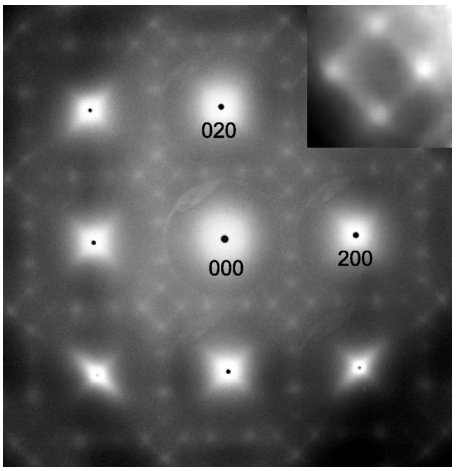

FIG. 2. Selected area electron diffraction pattern for the [100] zone axis of $Cu_{0.842}Al_{0.158}$ displaying diffuse scattering spots. The inset gives an enlargement of the four-fold splitting around the (110) reciprocal lattice point and shows the presence of weak diffuse streaks, which connect the diffuse scattering spots.

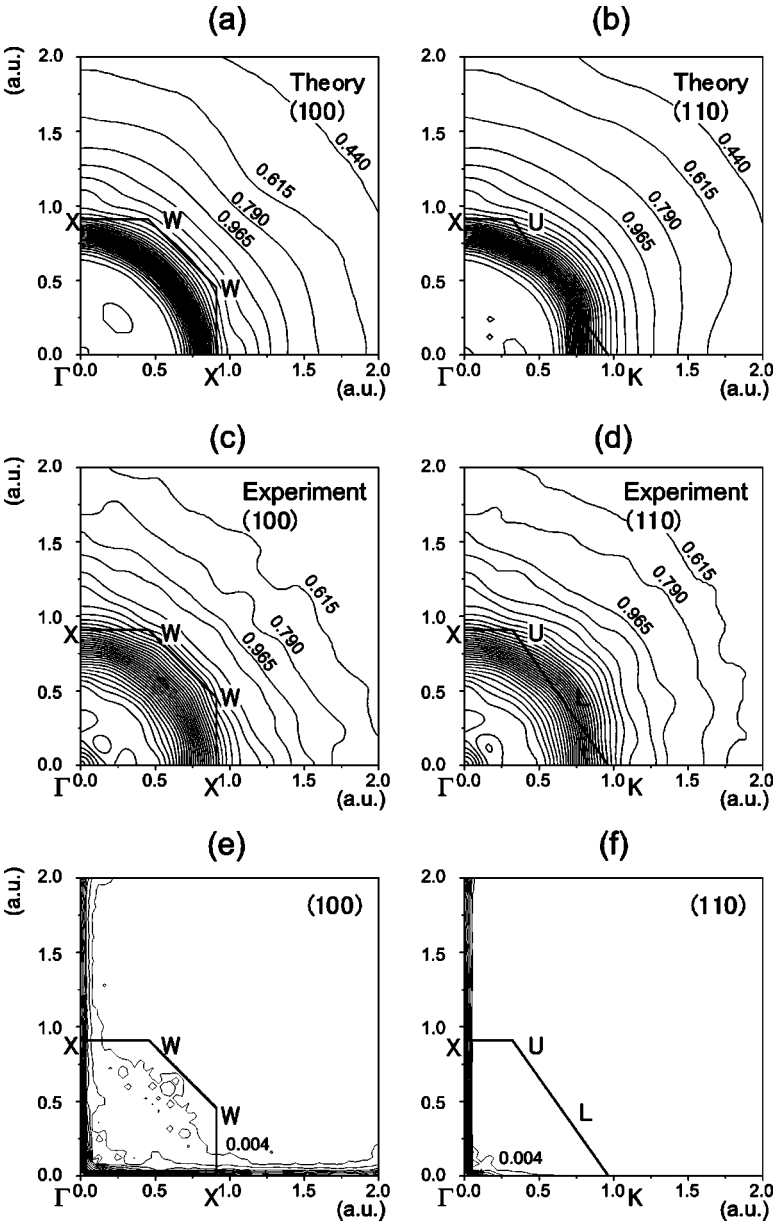

FIG. 3. (a)–(d) Theoretical and experimental contour maps of the reconstructed 3D momentum density of $Cu_{0.842}Al_{0.158}$ disordered alloy on the (100) and (110) planes. Boundary of the first Brillouin zone is marked. Contour step is 0.175 electrons/a.u.^{3}. (e) and (f) Error maps corresponding to the experimental plots in (c) and (d); contour step is 0.004 electrons/a.u.^{3}.

V. RESULTS AND DISCUSSION

We discuss diffuse scattering results first with reference to Fig. 2. The pattern of diffuse spots is easily seen to consist of fourfold and twofold splittings around the (110)- and (100)-type fcc superlattice positions, respectively. The inset further shows the presence of weak diffuse streaks connecting the four diffuse spots around the (110) superlattice position, which appear rather like the predictions of Ref. 19.[53] We are not aware of a previous observation of such streaks in CuAl alloys. Interestingly, Ohshima and Watanabe[42] and Rodewald *et al.*[43] report similar diffuse scattering patterns—four diffuse peaks connected by weak diffuse lines around (110)—in their electron diffraction studies of Cu-Pd alloys [see Fig. 1(b) of Ref. 42, and Figs. 1(b) and 1(c) of Ref. 43]. The intensity of the diffuse scattering detected by us in $Cu_{0.842}Al_{0.158}$ is, however, considerably lower than that observed for Cu-Pd.[54] Finally, as already pointed out, positions of diffuse scattering spots and the related connecting streaks can be used to determine specific FS dimensions; we return to this aspect of Fig. 2 below.

We turn now to consider the Compton scattering results. In this connection, the 3D momentum density $\rho_{\text{expt}}(\mathbf{p})$ was obtained by applying the reconstruction procedure described in Sec. III above to the 28 measured directional Compton profiles (CPs). In order to make a realistic comparison between theory and experiment, $\rho_{\text{theory}}(\mathbf{p})$ was similarly reconstructed from the 28 corresponding, computed CPs after folding in the experimental resolution broadening. In this way, effects of instrumental resolution as well as those of interpolation and filtering of very high frequency components generated during the Fourier transformation of Eq. (5) are incorporated properly in the theoretical momentum density.

Figure 3 compares $\rho_{\text{expt}}(\mathbf{p})$ and $\rho_{\text{theory}}(\mathbf{p})$ in the form of contour maps in two different planes in the momentum space

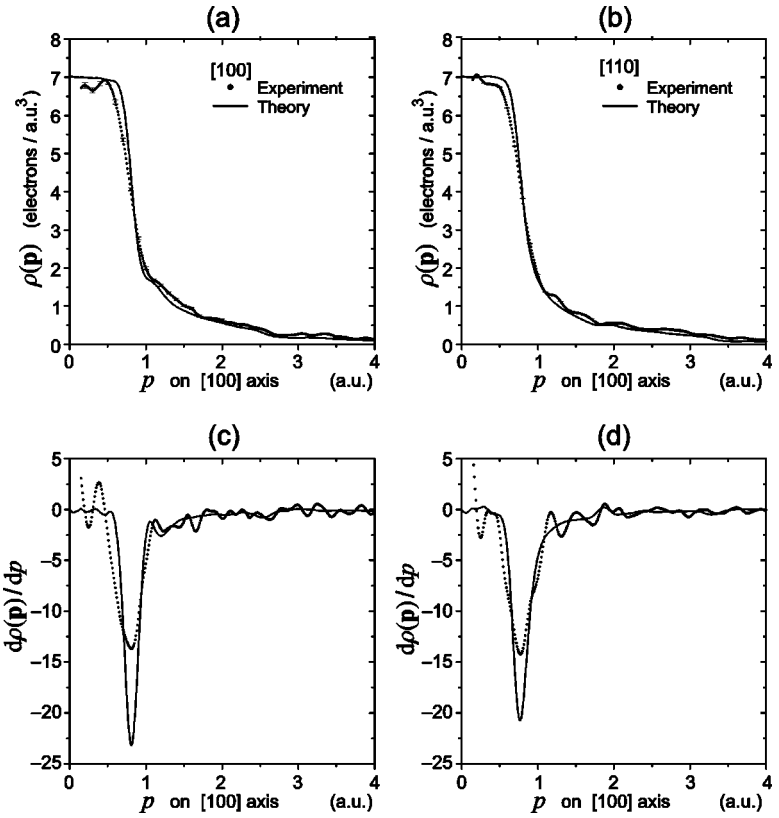

FIG. 4. Two typical sections through the 3D momentum density $\rho(\mathbf{p})$ and the corresponding first derivative $d\rho(\mathbf{p})/dp$ are shown. (a) and (c) are for the [100] direction, while (b) and (d) refer to the [110] direction. Full lines give the theoretical KKR-CPA results.

and shows a good overall level of accord, some discrepancies notwithstanding. From Figs. 3(a) and 3(c) we see that in the (100)-plane the theoretical and experimental contours are both quite circular in shape around the Γ-point. In sharp contrast, the contours in the (110)-plane in Figs. 3(b) and 3(d) are relatively flat along the Γ-K line, but are bulged along the Γ-L direction. Also notable is the bump due to the first higher momentum component just beyond 1.0 a.u. on the Γ-*X* axis in Figs. 3(a) and 3(c). These topological features are similar to those found previously in Cu (Ref. 44) and $Cu_{0.725}Pd_{0.275}$.[2]

The estimated errors in the reconstructed $\rho_{\text{expt}}(\mathbf{p})$ in the (100) and (110) planes are presented in the two bottom panels of Fig. 3. Referring to Fig. 3(e), the error distribution is seen to be strongly anisotropic. The largest error accumulation is at $\boldsymbol{p}=0$, with errors being generally large on the [100] axis and its immediate vicinity. These results are similar to those found in a study of a Cu-Pd alloy by Matsumoto *et al.*[2] and of Li by Tanaka *et al.*[3] According to the formula for the variance of $\rho(\mathbf{p})$ given by Tanaka *et al.*,[3] the main reason for the high accumulation of errors on the [100] axis is that this axis possesses the highest crystal symmetry.

The procedure for determining the FS is to first obtain the derivative $d\rho(\mathbf{p})/dp$ from $\rho(\mathbf{p})$, where $\boldsymbol{p}$ lies along various directions through the zone center. The Fermi momentum along any specific direction is then given by the position of the negative peak in $d\rho(\mathbf{p})/dp$, which defines the region of rapid variation of $\rho(\mathbf{p})$ separating filled and empty states. Figure 4, which considers [100] and [110] directions, provides illustrative examples. In order to avoid unnecessary confusion due to the aforementioned error accumulation near $\boldsymbol{p}=0$ [see Figs. 3(e) and 3(f)], the experimental momentum density is cut-off at $|\boldsymbol{p}|=0.15$ a.u. The appearance of ripples in $\rho(\mathbf{p})$ and $d\rho(\mathbf{p})/dp$, especially noticeable at high momenta, is an inevitable artifact, which results when one takes the Fourier transform of a discretely sampled dataset containing statistical errors. We have applied a slight convolution smoothing to the experimental CPs in order to suppress such ripples in the region of interest around the Fermi momenta, although care was taken to avoid worsening the resolution significantly. The excellent agreement seen between the positions of the experimental and theoretical (negative) Fermi surface peaks around 0.8 a.u. in Figs. 4(c) and 4(d) is typical of results along most directions in the Brillouin zone. The variation in $\rho(\mathbf{p})$, or equivalently the size of the dip in $d\rho(\mathbf{p})/dp$ in Fig. 4 around the Fermi momentum, is smoother in the experimental spectra compared to the theoretical predictions. Such an effect has been observed repeatedly in metals and alloys, e.g., Li,[1,3,4,45–48] Li-Mg,[5] Be,[49,50] and Al-Li,[6] and has been ascribed to the limited accuracy of the conventional local-density approximation based framework for describing electron correlations even in the simpler materials.

The final values of the Fermi surface radii, k_F, in the ΓXULK and ΓXWK planes are summarized in Fig. 5 for the investigated $Cu_{0.842}Al_{0.158}$ alloy sample. The corresponding results for Cu and Cu-rich Cu-Pd are shown for comparison (after Matsumoto *et al.*[2]).

Filled circles refer to the k_F data obtained from the reconstructed $\rho_{\text{expt}}(\mathbf{p})$ and the associated peaks in $d\rho(\mathbf{p})/dp$ from the present Compton spectra along the lines of the preceding paragraph. Interestingly, a similar analysis of $\rho_{\text{theory}}(\mathbf{p})$ yields a FS map, which is essentially indistinguishable in most directions from the filled circles, and for this reason it is not shown in order to avoid overcrowding the figure. We have

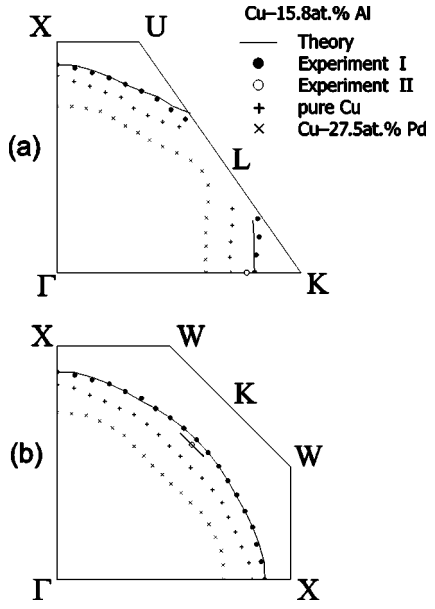

FIG. 5. Fermi surface of $Cu_{0.842}Al_{0.158}$ disordered alloy on the ΓXULK (a) and the ΓXWK (b) planes. Filled circles (Experiment I) give radii determined from the 3D momentum density reconstructed from the 28 experimental Compton profiles as discussed in the text. Theoretical KKR-CPA results are shown by the full line. Unfilled circle (Experiment II) denotes the (110) radius determined from the positions of the diffuse scattering spots; solid line attached to the open circle in (b) is based on the weak streaks connecting the diffuse spots (see inset to Fig. 2). For comparison, Fermi surface of Cu and of $Cu_{0.725}Pd_{0.275}$ disordered alloy, determined via Compton scattering measurements (after Ref. 2), are shown after normalizing the size of the Brillouin zone.

also computed the FS in $Cu_{0.842}Al_{0.158}$ more directly [without going through the reconstructed $\rho_{\text{theory}}(\mathbf{p})$] in terms of the positions of peaks in the KKR-CPA spectral density function A (k_F, E_F).[51,55] The theoretical FS so obtained (solid lines) is seen to be in remarkable agreement with the experimental Compton results. There are some discrepancies as one approaches the FS necks in the vicinity of the L-symmetry point, but these are not considered serious because the accuracy of the present procedure for determining the FS experimentally is not comparable to that of the theoretical procedure mentioned above. It is important to note that the FS radii given by the KKR-CPA spectral density function agree with those obtained from the computed CPs via the reconstructed momentum density $\rho_{\text{theory}}(\mathbf{p})$. This fact strongly justifies our procedure for obtaining the FS radii from the momentum density $\rho_{\text{expt}}(\mathbf{p})$ reconstructed using a series of Compton spectra.

As pointed out earlier, the diffuse scattering spots and the interconnecting streaks give imprints of the FS translated by the nesting vector. The FS caliper k_{F110} determined from the positions of the diffuse scattering spots in our electron diffraction pattern (see Fig. 2) is plotted in Fig. 5 as an open circle. The FS radii in the close proximity of k_{F110} in the ΓXWK plane can be adduced from the weak connecting streaks in the electron diffraction pattern as indicated by the short solid line attached to the open circle. Our k_{F110} diffuse scattering value of 0.745 ± 0.005 a.u. is in very good agreement with the value of 0.740 a.u. obtained for $Cu_{84}Al_{16}$ by Scattergood *et al.*,[22] but it is smaller than the value determined from Compton spectra or the KKR-CPA computations. The reason for this slight discrepancy is not clear.

Figure 5 makes it clear that the FS of Cu does not simply inflate or deflate uniformly when electrons are added or subtracted by alloying, but that changes in the electron/atom ratio are accompanied by substantial changes in the shape of the FS. Upon the addition of Pd, the FS of Cu becomes flatter along the Γ-K direction as it decreases in size. This however is not the case when Al is alloyed into Cu and the size of the FS grows. The FS of $Cu_{0.842}Al_{0.158}$ is seen to be less flat along Γ-K compared to that of $Cu_{0.725}Pd_{0.275}$. It follows that the associated peak in the susceptibility arising from the nesting of the FS along Γ-K will be weaker in CuAl compared to CuPd alloys. Interestingly, this result is at least qualitatively consistent with our observation that the intensity of diffuse scattering spots in our measurements was found to be extremely weak.

In conclusion, we have measured high resolution Compton profiles along a series of 28 independent directions from $Cu_{0.842}Al_{0.158}$ disordered alloy single crystals with normals to the surfaces oriented along the [100], [110], and [111] directions and used these data to reconstruct the 3D momentum density $\rho_{\text{expt}}(\mathbf{p})$. In order to help interpret these experimental results, parallel first-principles KKR-CPA computations of the corresponding 28 profiles have been carried out. The Fermi surface in $Cu_{0.842}Al_{0.158}$ determined from the Compton data in the (100) and (110) planes is found to be in good agreement with the KKR-CPA predictions. An electron diffraction study of the present $Cu_{0.842}Al_{0.158}$ sample was additionally undertaken. The scattering pattern displayed fourfold splitting around the (110)-type fcc superlattice positions indicating short-range ordering effects in the alloy. Moreover, weak streaks connecting the four diffuse scattering spots around (110) were observed—to our knowledge for the first time in Cu-Al. An examination of changes in the shape of the Fermi surface with alloying and the intensity of diffuse scattering spots relative to that of the main diffraction peaks, leads us to conclude that this study on Cu-Al solid solutions is consistent with the notion that Fermi surface nesting is an important factor in driving short-range ordering in disordered alloys.

ACKNOWLEDGMENTS

The authors are grateful to Steve Dugdale and Bob Markiewicz for fruitful discussions. The measurements of the Compton profiles were carried out with the approval of the Photon Factory Advisory Committee, Proposal Nos. 97-G288 and 99G144. The authors thank the Polish Committee for Scientific Research for supporting Polish-Japanese cooperation, Project No. R108. This work is supported in part by the US Department of Energy contract DE-AC03-76SF00098, and benefited from the allocation of supercomputer time at the NERSC and the Northeastern University's Advanced Scientific Computation Center (ASCC).

[1] Y. Sakurai, Y. Tanaka, A. Bansil, S. Kaprzyk, A. T. Stewart, Y. Nagashima, T. Hyodo, S. Nanao, H. Kawata, and N. Shiotani, Phys. Rev. Lett. **74**, 2252 (1995).
[2] I. Matsumoto, H. Kawata, and N. Shiotani, Phys. Rev. B **64**, 195132 (2001).
[3] Y. Tanaka, Y. Sakurai, A. T. Stewart, N. Shiotani, P. E. Mijnarends, S. Kaprzyk, and A. Bansil, Phys. Rev. B **63**, 045120 (2001).
[4] W. Schülke, G. Stutz, F. Wohlert, and A. Kaprolat, Phys. Rev. B **54**, 14 381 (1996).
[5] G. Stutz, F. Wohlert, A. Kaprolat, W. Schülke, Y. Sakurai, Y. Tanaka, M. Ito, H. Kawata, N. Shiotani, S. Kaprzyk, and A. Bansil, Phys. Rev. B **60**, 7099 (1999).
[6] I. Matsumoto, J. Kwiatkowska, F. Maniawski, M. Itou, H. Kawata, N. Shiotani, S. Kaprzyk, P. E. Mijnarends, B. Barbiellini, and A. Bansil, Phys. Rev. B **64**, 045121 (2001).
[7] S. B. Dugdale, H. M. Fretwell, M. A. Alam, G. Kontrym-Sznajd, R. N. West, and S. Badrzadeh, Phys. Rev. Lett. **79**, 941 (1997).
[8] H. M. Fretwell, S. B. Dugdale, M. A. Alam, D. C. R. Hedley, A. Rodriguez-Gonzalez, and S. B. Palmer, Phys. Rev. Lett. **82**, 3867 (1999).
[9] S. B. Dugdale, M. A. Alam, I. Wilkinson, R. J. Hughes, I. R. Fisher, P. C. Canfield, T. Jarlborg, and G. Santi, Phys. Rev. Lett. **83**, 4824 (1999).
[10] I. Wilkinson, R. J. Hughes, Zs. Major, S. B. Dugdale, M. A. Alam, E. Bruno, B. Ginatempo, and E. S. Giuliano, Phys. Rev. Lett. **87**, 216401 (2001).
[11] M. Samsel-Czekała, G. Kontrym-Sznajd, G. Döring, W. Schülke, J. Kwiatkowska, F. Maniawski, S. Kaprzyk, and A. Bansil, Appl. Phys. A: Mater. Sci. Process. **76**, 87 (2003).
[12] W. Kohn, Phys. Rev. Lett. **2**, 393 (1959).
[13] W. M. Lomer, Proc. Phys. Soc. Jpn. **80**, 489 (1962).
[14] W. M. Lomer, Proc. Phys. Soc. Jpn. **84**, 327 (1964).
[15] M. Tachiki and K. Teramoto, J. Phys. Chem. Solids **27**, 335 (1966).
[16] P. C. Clapp and S. C. Moss, Phys. Rev. **142**, 418 (1966).
[17] P. C. Clapp and S. C. Moss, Phys. Rev. **171**, 754 (1968).
[18] S. C. Moss and P. C. Clapp, Phys. Rev. **171**, 764 (1968).
[19] S. C. Moss, Phys. Rev. Lett. **22**, 1108 (1969).
[20] B. L. Gyorffy and G. M. Stocks, Phys. Rev. Lett. **50**, 374 (1983).
[21] B. Borie and C. J. Sparks, Acta Crystallogr. **17**, 827 (1964).
[22] R. O. Scattergood, S. C. Moss, and M. B. Bever, Acta Metall. **18**, 1087 (1970).
[23] J. E. Epperson, P. Fuernrohr, and C. Ortiz, Acta Crystallogr., Sect. A: Cryst. Phys., Diffr., Theor. Gen. Crystallogr. **34**, 667 (1978).
[24] K. Fujiwara, O. Sueoka, and T. Imura, J. Phys. Soc. Jpn. **24**, 467 (1968).
[25] A. Thompson, B. M. Murray, and S. Berko, Phys. Lett. **37A**, 461 (1971).
[26] T. Akahane, O. Sueoka, H. Morinaga, and K. Fujiwara, J. Phys. Soc. Jpn. **36**, 135 (1974).
[27] S. Berko and J. Mader, Appl. Phys. **5**, 287 (1975).
[28] H. Asonen, M. Lindroos, M. Pessa, R. Prasad, R. S. Rao, and A. Bansil, Phys. Rev. B **25**, 7075 (1982).
[29] Y. Sakurai, M. Ito, T. Urai, Y. Tanaka, N. Sakai, T. Iwazumi, H. Kawata, M. Ando, and N. Shiotani, Rev. Sci. Instrum. **63**, 1190 (1992).
[30] N. Sakai, J. Phys. Soc. Jpn. **56**, 2477 (1987).
[31] R. Suzuki, M. Osawa, S. Tanigawa, M. Matsumoto, and N. Shiotani, J. Phys. Soc. Jpn. **58**, 3251 (1989).
[32] Y. Tanaka, N. Sakai, Y. Kubo, and H. Kawata, Phys. Rev. Lett. **70**, 1537 (1993).
[33] M. Ito and Y. Amemiya, Nucl. Instrum. Methods Phys. Res. A **310**, 369 (1991).
[34] A. Bansil, S. Kaprzyk, and J. Toboła, in *Application of Multiple Scattering Theory to Materials Science*, edited by W. H. Butler, P. H. Dedericks, A. Gonis, and R. Weaver (Materials Research Society, Pittsburgh, 1992).
[35] A. Bansil, S. Kaprzyk, P. E. Mijnarends, and J. Toboła, Phys. Rev. B **60**, 13 396 (1999) and references therein.
[36] S. Kaprzyk and A. Bansil, Phys. Rev. B **42**, 7358 (1990).
[37] A. Bansil and S. Kaprzyk, Phys. Rev. B **43**, 10 335 (1991).
[38] See, e.g., A. Gonis, *Green Functions for Ordered and Disordered Systems*, Vol. 4 of Studies in Mathematical Systems (North-Holland, Amsterdam, 1992).
[39] P. E. Mijnarends and A. Bansil, Phys. Rev. B **13**, 2381 (1976).
[40] A. Bansil, R. S. Rao, P. E. Mijnarends, and L. Schwartz, Phys. Rev. B **23**, 3608 (1981).
[41] U. von Barth and L. Hedin, J. Phys. C **5**, 1629 (1972).
[42] K. Ohshima and D. Watanabe, Acta Crystallogr., Sect. A: Cryst. Phys., Diffr., Theor. Gen. Crystallogr. **A29**, 520 (1973).
[43] M. Rodewald, K. Rodewald, P. De Meulenaere, and G. Van Tendeloo, Phys. Rev. B **55**, 14 173 (1997).
[44] Y. Kubo, Y. Sakurai, and N. Shiotani, J. Phys.: Condens. Matter **11**, 1683 (1999).
[45] Y. Kubo, J. Phys. Soc. Jpn. **66**, 2236 (1997).
[46] W. Schülke, J. Phys. Soc. Jpn. **68**, 2470 (1999).
[47] C. Filippi and D. M. Ceperley, Phys. Rev. B **59**, 7907 (1999).
[48] B. Barbiellini and A. Bansil, J. Phys. Chem. Solids **62**, 2181 (2001).
[49] M. Y. Chou, P. K. Lam, M. L. Cohen, G. Loupias, J. Chomilier, and J. Petiau, Phys. Rev. Lett. **49**, 1452 (1982).
[50] M. Itou, Y. Sakurai, T. Ohata, A. Bansil, S. Kaprzyk, Y. Tanaka, H. Kawata, and N. Shiotani, J. Phys. Chem. Solids **59**, 99 (1998).
[51] A. Bansil, Phys. Rev. B **20**, 4035 (1979).
[52] The Compton scattering cross-section is proportional to the Compton profile. Therefore, anisotropy of the Compton profile (at most a few percent at the Compton peak) yields a negligible anisotropic contribution in the processes of Compton scattering followed by another Compton scattering. More importantly, the thickness and hence the effective path length for photons is different for different directions of the scattering vector, which induces an anisotropy in the cross-section for double scattering events. This effect however is included in our Monte Carlo simulations.
[53] See, e.g., Fig. 2 of Ref. 19.
[54] The limitation inherent in the electron diffraction method is that quantitative comparison between different patterns is difficult to make. Our argument here is, therefore, based on qualitative assessment of intensities typically observed in electron diffraction patterns for and CuAl alloys.
[55] When $A(k,E_F)$ is plotted as a funtion of k at E_F, the spectral peaks possess a finite width Δk, which reflects the disorder induced smearing of the FS. However, our KKR-CPA estimates indicate that the size of Δk in $Cu_{0.842}Al_{0.158}$ is typically much less than the momentum resolution of our Compton experiments.